UNIVERSITY
OF TRENTO

DIPARTIMENTO DI INGEGNERIA E SCIENZA DELL'INFORMAZIONE

38123 Povo – Trento (Italy), Via Sommarive 14
http://www.disi.unitn.it

SYNTHESIS OF METAMATERIAL-ENHANCED RADIATING
DEVICES

E. T. Bekele, F. Viani, L. Manica, and Douglas H. Werner

October 2012

Technical Report # DISI-12-037

Contents

1 Introduction

This report presents description of the qTO software package. The application of the software is demonstrated with an example test case provided with the software. An additional test case considering theoretical Transformation Electromagnetics is also reported.

2 Description of the qTO software

The software package implements a quasi-conformal transformation (qTO) in two dimensions. In its canonical application, polygons in virtual plane are transformed to rectangular regions in the physical plane. The polygon in the virtual plane is expected to have a constant material properties (ε_r, μ_r) and the software computes the material properties in the rectangular region that can support equivalent electromagnetic properties. The reverse transformation from a rectangle in virtual plane to polygon in physical plane is also supported but material properties are not computed in this case.

The software is organized as a package qTO and the core of the software is the class *Transformation*. This class contains routines (methods) to perform "normal" and inverse transformations. The normal transformation is implemented by the function *Transformation.build(path,cornerpoints,gridx,varargin)*. The argument *path* defines the (x, y) coordinates of the boundary of the virtual polygon. In the construction of the shape, consecutive points in *path* are joined by straight line, therefore curved regions need to be sampled more densely. A grid is generated(How?) in the virtual and physical planes, and the software requires four(Why four? Which four?) corners of the polygon as input for grid generation. The argument *cornerpoints* defines these corners. The inverse mapping is implemented in the function *T.Inverse()*. In addition, the package contains extensive tools for graphical output.

3 Example 1: Double Convex Lens

This example is included with the software as a demonstration. The example includes design of a Transformation Optics (TO) flat biconvex lens extended with a box (in the sense of optical focusing).

3.1 Virtual Object parameters:

The classical constant refractive index (constant ε_r and μ_r) lens (in the virtual plane) has the following parameters:

- Radius of curvature: $r = 50$ (arbitrary units)

- Lens Width: $w = 30$(arbitrary units)

- Lens thickness at corner: $t = 5$ (arbitrary units)

- Lens angle: $thb = 15^0$

- Relative permittivity: $\varepsilon_r = 4$

- Non-magnetic lens: $\mu_r = 1$

3.2 Result and Discussion

The result of the transformation is described as follows. Figure 1 shows geometries and grids in virtual(top) and physical(bottom) plane. It is stated that quasi conformal mapping perturbs orthogonality of the grid(How?). This means accuracy of isotropic medium approximation is reduced(How?). It is also stated that this effect is small and can be neglected. Additional figures are provided to demonstrate that the effect of the perturbation is "small" and can be neglected. Towards this end, Figure 4 shows the fraction of grid intersections that deviate from orthogonality. It can be seen that very few fraction of entries deviate from orthogonality. Figure 5 shows the actual material properties, with no isotropic approximation. The off-diagonal entries in this figure (e_{xy}) are approximately zero nearly throughout the rectangle, hence can be "reasonably" approximated to be constant zero. Values for e_{xx} and e_{yy} are nearly constant throughout the region and the only main variation is observed in e_{zz}. Therefore the isotropic approximation is "reasonably" accurate.
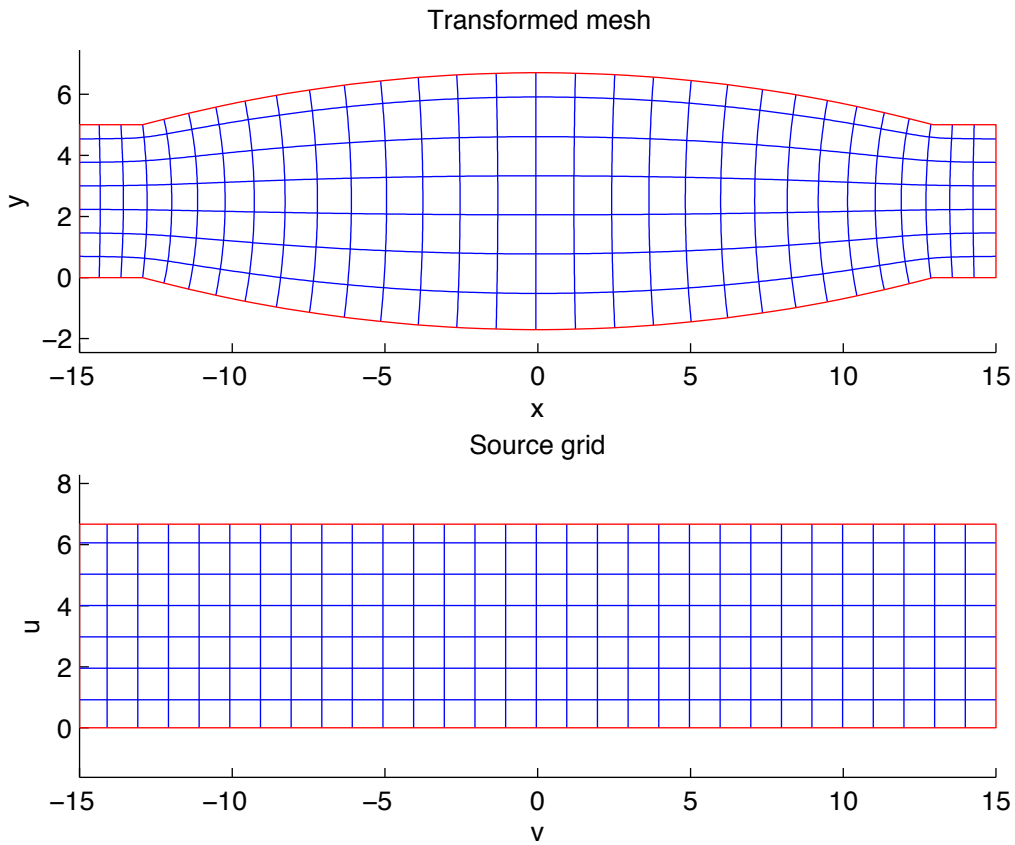
Transformed mesh

Source grid

Figure 1: qTO transformation of biconvex lens: Transformed(virtual plane) and Source(physical plane) grids.

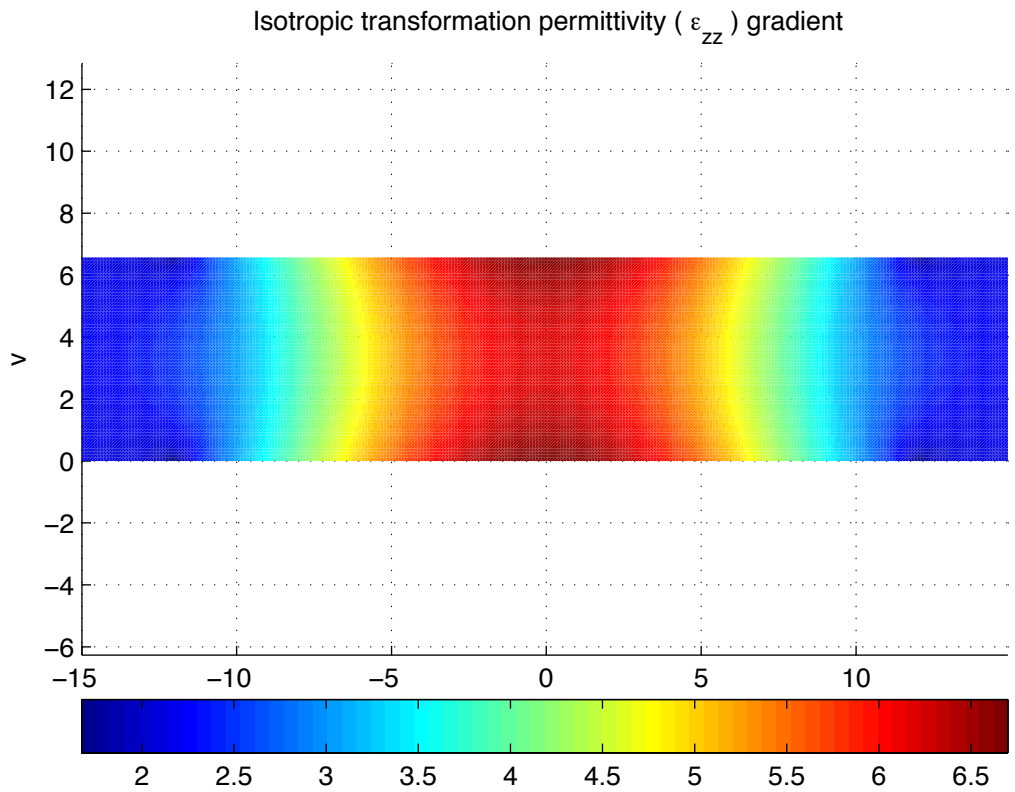## Isotropic transformation permittivity (ε_{zz}) gradient

Figure 2: qTO transformation of biconvex lens: Isotropic transformation relative permittivity e_{zz} in the physical plane.
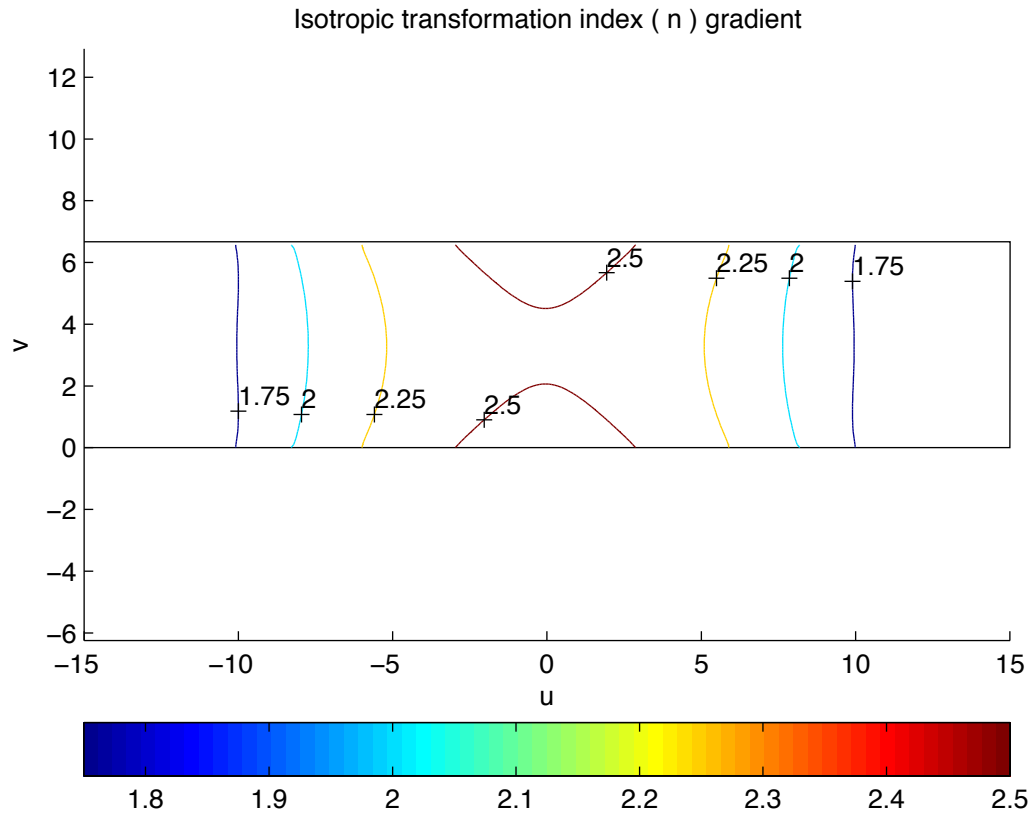
Figure 3: qTO transformation of biconvex lens: Isotropic transformation Refractive index, (n), gradient in the physical plane.
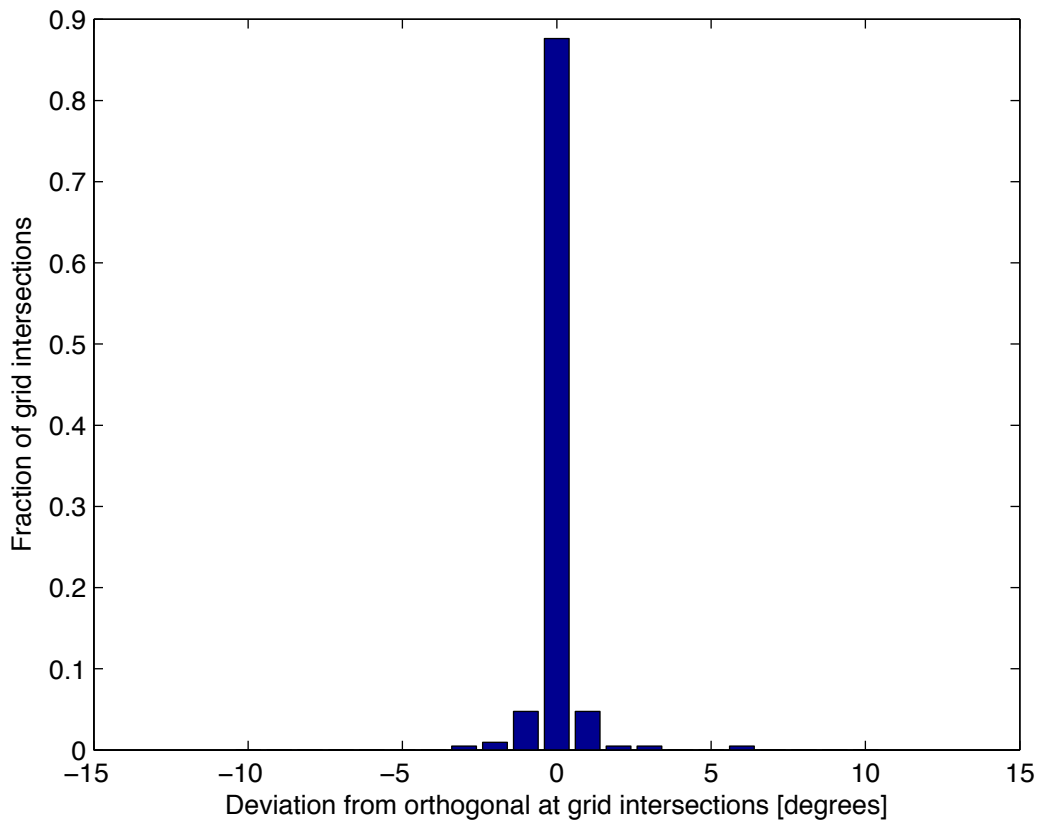

Figure 4: qTO transformation of biconvex lens: Isotropic transformation grid orthogonality test
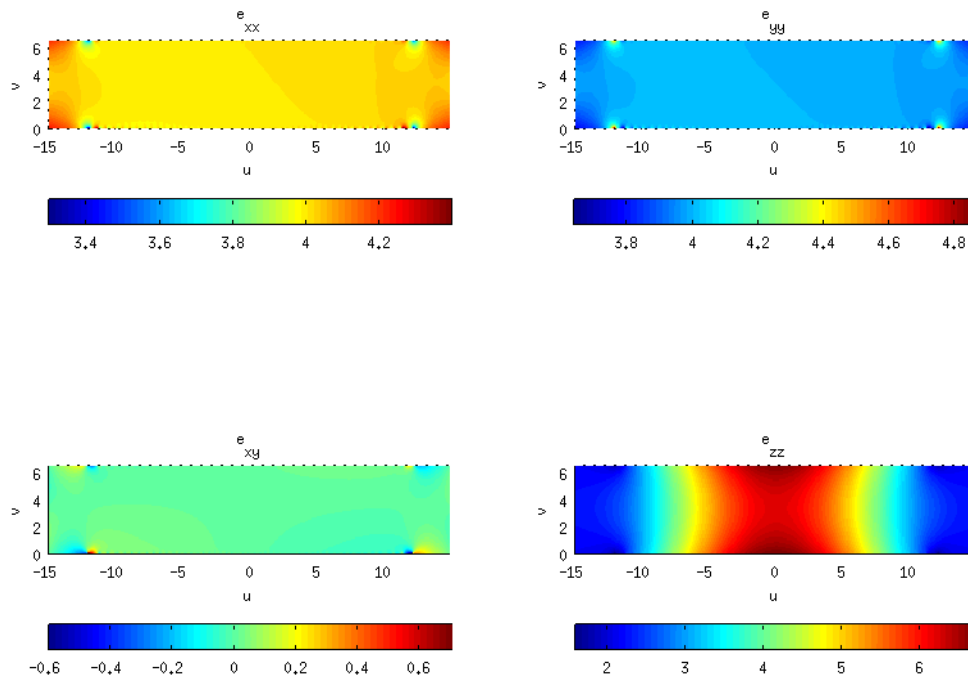
Figure 5: qTO transformation of biconvex lens: Anisotropic transformation relative permittivity in the physical plane.

4   Example 2: Field Concentrator

To demonstrate use of the software package in the context of transformation electromagnetics (TE), an example different from the one provided with the software is considered. Here a synthesis of theoretical field concentrator is attempted based on the a simple coordinate transformation example provided in [1]. In the virtual plane, the propagation medium is constricted at its center and the wave is forced to traverse this narrow region. The geometry of the proposed virtual object is shown in Figure 6.
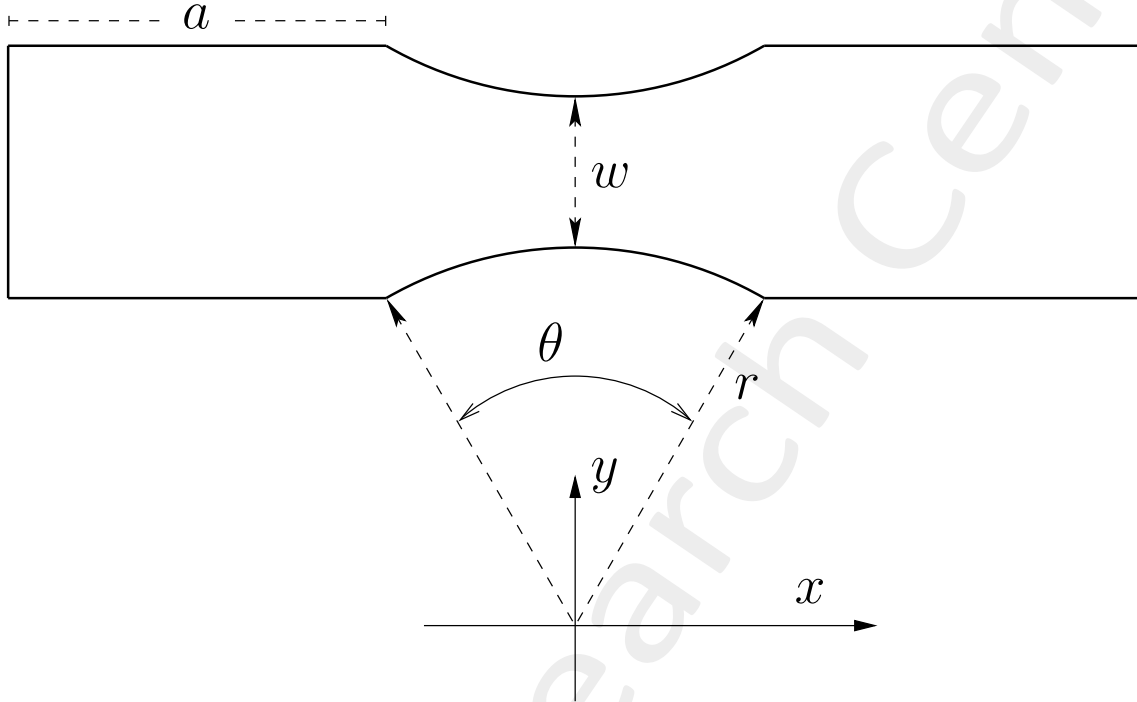

Figure 6: qTO transformation of field concentrator: Geometry of proposed virtual structure.

4.1   Virtual Object parameters:

With reference to the labels in Figure 6, the virtual object is parametrized as follows:

- Radius : $r = 50$ (arbitrary units)

- $w = 20$ (arbitrary units)

- $a = 50$ (arbitrary units)

- Arc angle: $\theta = 60^0$

- Constant relative permittivity: $\varepsilon_r = 4$

- Non-magnetic medium: $\mu_r = 1$

4.2   Result and Discussion

The transformation was peformed mimicking the previous example, and the result of the transformation are presented as follows. Figure 7 shows the transformation grid in both physical and virtual planes. Figure 8 reports medium permittivity for with isotropic approximation. The gradient of the refractive index is reported in Figure 9. When compared to the previous example (Figure 4 vs Figure 10), one can see that the fraction of non-orthogonal grid crossings has increased. The exact (anisotropic) medium parameters are reported in Figure 11. Also in this case, e_{xy} component of the relative permittivity tensor has near zero values throughout most the region of interest. Similarly, the components e_{xx} and e_{yy} are almost constant and the isotropic approximation can be considered accurate.
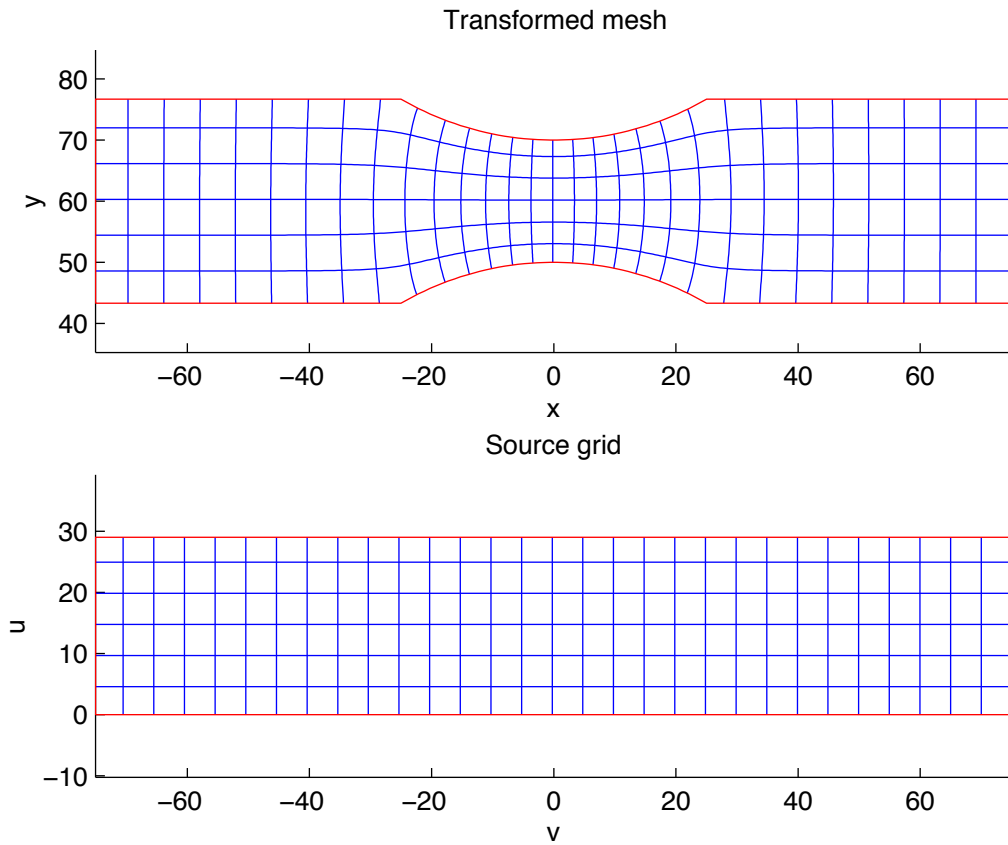
Figure 7: qTO transformation of field concentrator: Transformed(virtual plane) and Source(physical plane) grids.
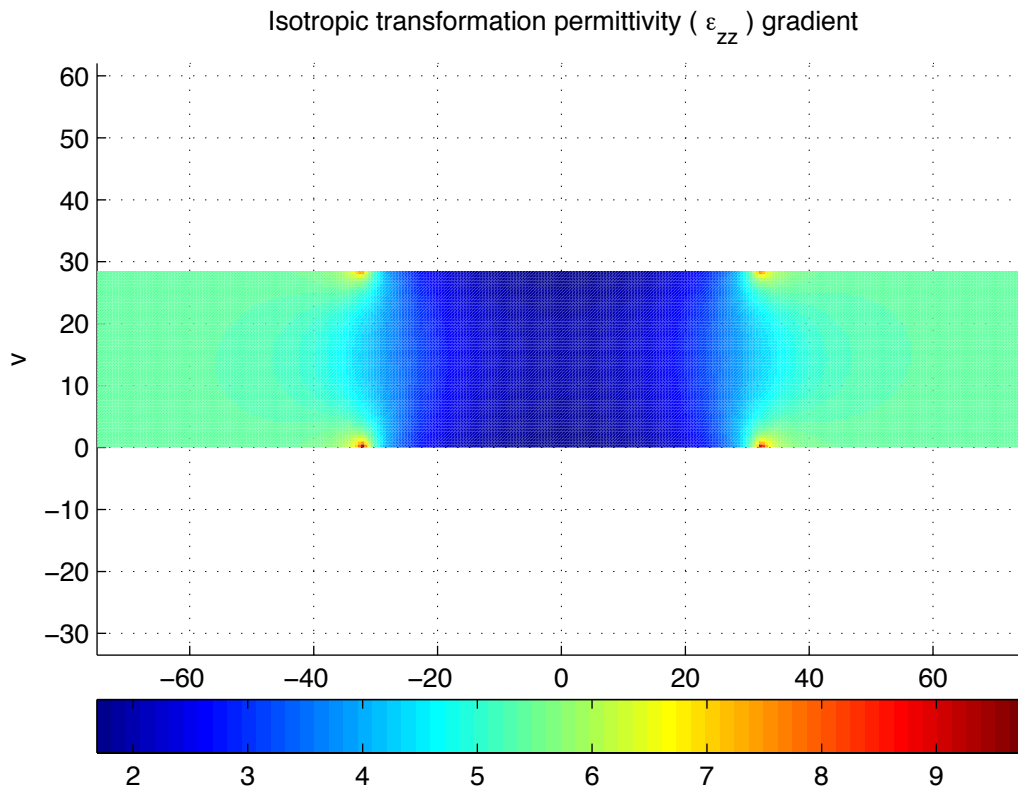

Figure 8: qTO transformation of field concentrator: Isotropic transformation relative permittivity e_{zz} in the physical plane.
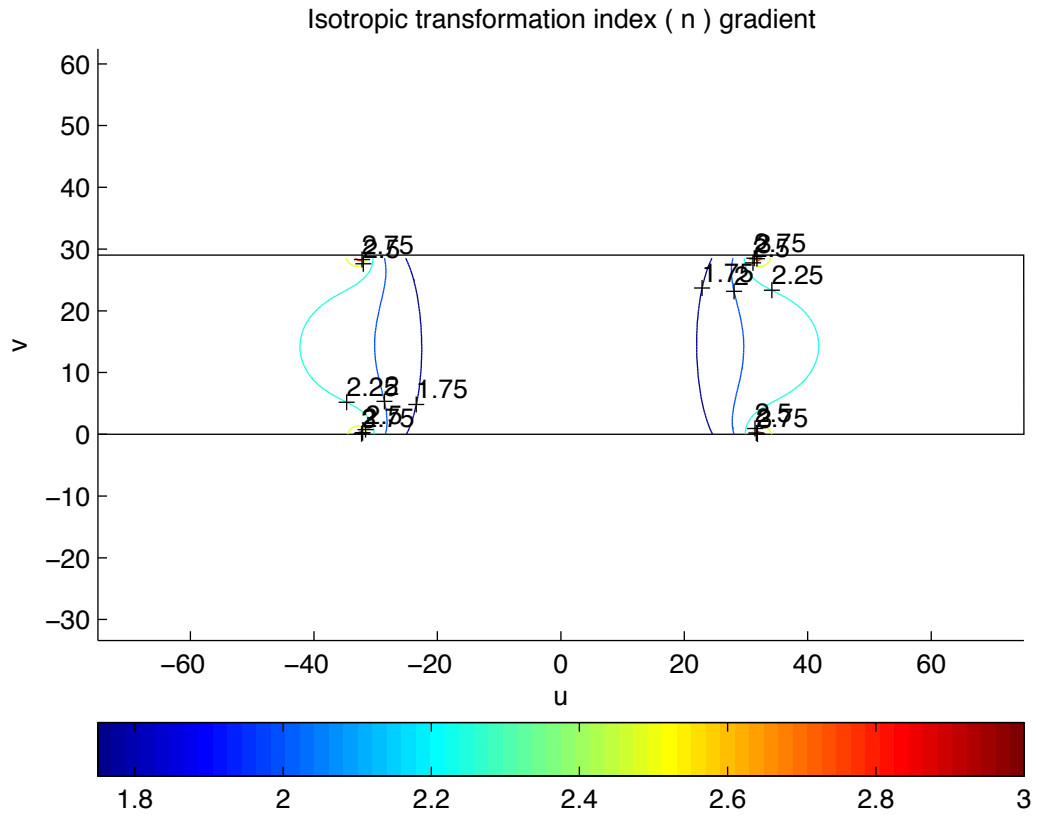
Figure 9: qTO transformation of field concentrator: Isotropic transformation Refractive index, (n), gradient in the physical plane.
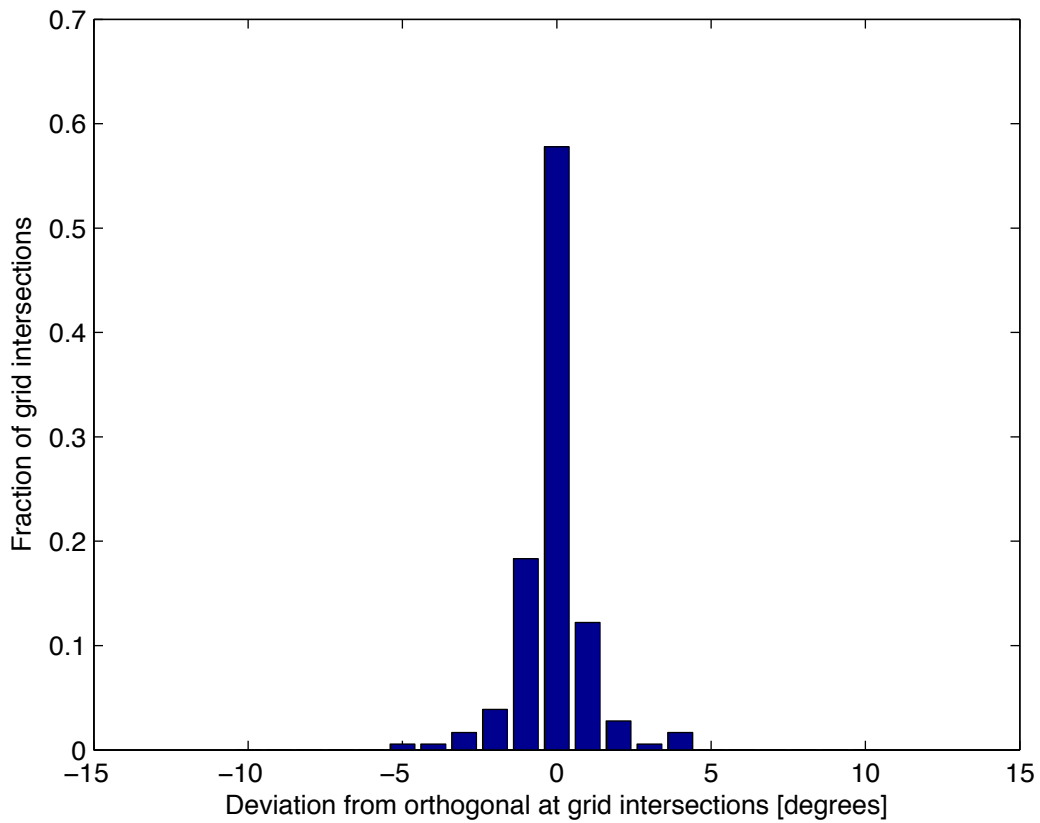

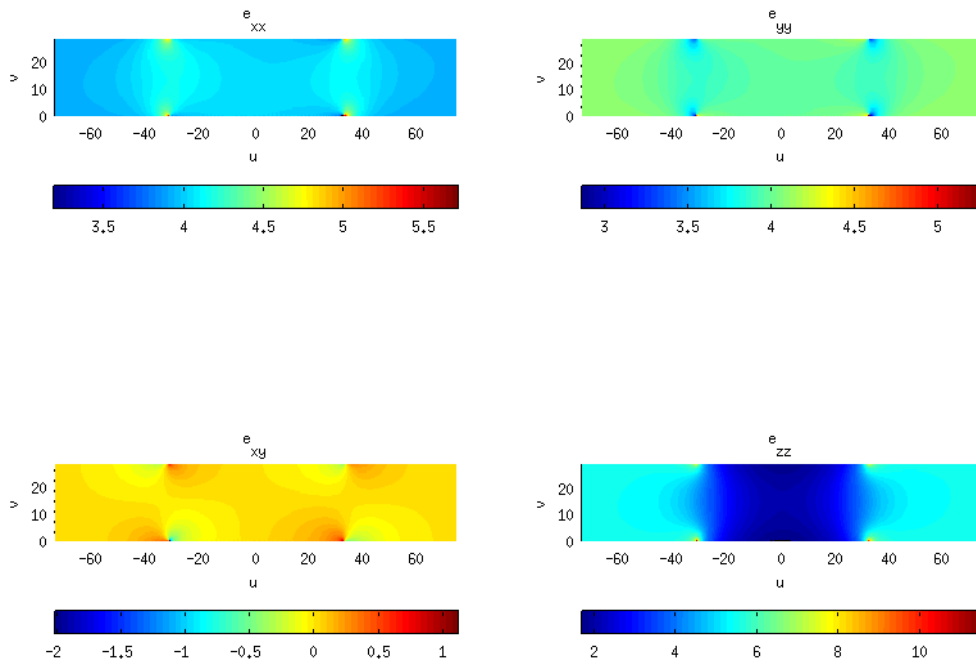**Figure 10:** qTO transformation of field concentrator: Isotropic transformation grid orthogonality test

Figure 11: qTO transformation of field concentrator: Anisotropic transformation relative permittivity in the physical plane.

Acknowledgment

References

[1] D.-H. Kwon and D. H. Werner, "Transformation electromagnetics: An overview of the theory and applications," *IEEE Antennas Propag. Mag.*, vol. 52, no. 1, pp. 24-26, Feb. 2010.

[2] P. Rocca, M. Benedetti, M. Donelli, D. Franceschini, and A. Massa, "Evolutionary optimization as applied to inverse problems," Inverse Problems - 25th Year Special Issue of Inverse Problems, Invited Topical Review, vol. 25, pp. 1-41, Dec. 2009.

[3] P. Rocca, G. Oliveri, and A. Massa, "Differential Evolution as applied to electromagnetics," IEEE Antennas and Propagation Magazine, vol. 53, no. 1, pp. 38-49, Feb. 2011.

[4] G. Oliveri and A. Massa, "GA-Enhanced ADS-based approach for array thinning," IET Microwaves, Antennas & Propagation , vol. 5, no. 3, pp. 305-315, 2011.

[5] G. Oliveri, F. Caramanica, and A. Massa, "Hybrid ADS-based techniques for radio astronomy array design," IEEE Transactions on Antennas and Propagation - Special Issue on "Antennas for Next Generation Radio Telescopes," vol. 59, no. 6, pp. 1817-1827, Jun. 2011.

[6] L. Poli, P. Rocca, G. Oliveri, and A. Massa, "Harmonic beamforming in time-modulated linear arrays," IEEE Transactions on Antennas and Propagation, vol. 59, no. 7, pp. 2538-2545, Jul. 2011.

[7] L. Poli, P. Rocca, L. Manica, and A. Massa, "Handling sideband radiations in time-modulated arrays through particle swarm optimization," IEEE Transactions on Antennas and Propagation, vol. 58, no. 4, pp. 1408-1411, Apr. 2010.

[8] L. Poli, P. Rocca, L. Manica, and A. Massa, "Time modulated planar arrays - Analysis and optimization of the sideband radiations," IET Microwaves, Antennas & Propagation, vol. 4, no. 9, pp. 1165-1171, 2010.

[9] L. Lizzi, F. Viani, R. Azaro, and A. Massa, "Optimization of a spline-shaped UWB antenna by PSO," IEEE Antennas and Wireless Propagation Letters, vol. 6, pp. 182-185, 2007.

[10] L. Lizzi, F. Viani, R. Azaro, and A. Massa, "A PSO-driven spline-based shaping approach for ultra-wideband (UWB) antenna synthesis," IEEE Transactions on Antennas and Propagation, vol. 56, no. 8, pp. 2613-2621, Aug. 2008.

[11] P. Rocca, L. Manica, and A. Massa, "An improved excitation matching method based on an ant colony optimization for suboptimal-free clustering in sum-difference compromise synthesis," IEEE Transactions on Antennas and Propagation, vol. 57, no. 8, pp. 2297-2306, Aug. 2009.

[12] P. Rocca, L. Manica, and A. Massa, "Ant colony based hybrid approach for optimal compromise sum-difference patterns synthesis," Microwave and Optical Technology Letters, vol. 52, no. 1, pp. 128-132, Jan. 2010.

[13] P. Rocca, L. Manica, F. Stringari, and A. Massa, "Ant colony optimization for tree-searching based synthesis of monopulse array antenna," Electronics Letters, vol. 44, no. 13, pp. 783-785, Jun. 19, 2008.

[14] G. Oliveri and L. Poli, "Optimal sub-arraying of compromise planar arrays through an innovative ACO-weighted procedure," Progress in Electromagnetic Research, vol. 109, pp. 279-299, 2010.

[15] G. Oliveri, "Improving the reliability of frequency domain simulators in the presence of homogeneous metamaterials â A preliminary numerical assessment," Progress In Electromagnetics Research, vol. 122, pp. 497-518, 2012.